Tumor Cell–Secreted Caveolin-1 Has Proangiogenic Activities in Prostate Cancer

Salahaldin A. Tahir,[1] Guang Yang,[1] Alexei A. Goltsov,[1] Masami Watanabe,[1] Ken-ichi Tabata,[1] Josephine Addai,[1] El Moataz Abdel Fattah,[1] Dov Kadmon,[1] and Timothy C. Thompson[1,2,3]

[1]Scott Department of Urology, Departments of [2]Molecular and Cellular Biology and [3]Radiology, Baylor College of Medicine, Houston, Texas

Abstract

Caveolin, a major structural component of specialized plasma membrane invaginations (caveolae) that participate in diverse cellular activities, has been implicated in the pathogenesis of several human diseases, including cancer. We showed in earlier studies that caveolin-1 (cav-1) is consistently and strongly overexpressed in metastatic prostate cancer and is secreted in a biologically active form by virulent prostate cancer cells. Using both *in vitro* and *in vivo* model systems, we now present evidence supporting a proangiogenic role for cav-1 in prostate cancer development and progression. Recombinant cav-1 (rcav-1) was taken up by cav-1$^{-/-}$ endothelial cells through either a lipid raft/caveolae- or clathrin-dependent mechanism, leading to specific angiogenic activities (tubule formation, cell migration, and nitric oxide production) that were mediated by rcav-1 stimulation of the PI3K-Akt-eNOS signaling module. Pathologic angiogenesis induced by cav-1 in prostate cancer–bearing mice correlated with an increased frequency, number, and size of lung metastases. We propose that in addition to its antiapoptotic role, cav-1 secreted by prostate cancer cells functions critically as a proangiogenic factor in metastatic progression of this tumor. These new insights into cav-1 function in prostate cancer may provide a base for the design of clinically applicable therapeutic strategies. [Cancer Res 2008;68(3):731–9]

Introduction

As essential components of caveolae, caveolin proteins help to generate and maintain these highly ordered structures at the cell surface. They also mediated endocytosis and transcytosis of molecules attached to the cell surface and organize signaling proteins involved in cell proliferation, adhesion, and migration, among numerous other biological processes (1). This functional versatility has focused increasing attention on the possible role of caveolins in cancer development and progression. Findings to date clearly indicate that caveolin-1 (cav-1), the first of several caveolin family members that differ in structure and tissue distribution, can influence both tumorigenesis and metastatic spread in certain types of cancer (2–6), although the mechanisms of these effects are largely unknown. We showed in earlier studies that cav-1 is consistently and strongly overexpressed in metastatic prostate cancer and is secreted in a biologically active form by virulent prostate cancer cells (2, 3, 7). Interestingly, we detected significantly increased serum cav-1 levels in prostate cancer patients compared with control men or men with benign prostatic hyperplasia, and showed that preoperative serum cav-1 is a potential prognostic marker for recurrence in radical prostatectomy cohort (8, 9). The ability of some prostate cancer cells to secrete biologically active cav-1 (7, 8), and the demonstration that loss of cav-1 function in the TRAMP transgenic mouse prostate cancer model results in highly significant reductions of prostate cancer growth and metastasis (10), led us to suspect that tumor cell–secreted cav-1 may function as a paracrine factor during prostate cancer development, possibly as a regulator of pathologic angiogenesis. The studies described here substantiate this role and suggest a paradigm that may be applicable to other tumors that secrete cav-1.

Materials and Methods

Endothelial cell isolation. Endothelial cells from *cav-1*$^{-/-}$ mice (11) were isolated from mouse aorta according to the primary explant procedure and used throughout the study. Briefly, the aorta was removed from the anaesthetized mice, placed in PBS, and carefully cleaned of periadventitial fat and connective tissue. The vessel was then cut into 1-mm pieces, opened longitudinally, and placed with the intima side down on Matrigel-coated (BD Biosciences) 12-well plates in endothelial cell growth medium (EGM; Cambrex) to generate endothelial outgrowth. The aortic pieces were removed after 4 to 7 days, and the cells were allowed to grow to confluence. After recovery with dispase, the cells were plated on a 12-well plate and then subcultured twice. The confluent monolayers showed the typical cobblestone pattern of endothelial cells stained positively for uptake of Dil-Ac-LDL (Biomedical Technologies).

Western blotting. Protein aliquots from cell lysates were separated by 10% or 12% SDS-PAGE and transferred to nitrocellulose membranes. The membranes were probed with antibodies to cav-1 (Santa Cruz Biotechnology), eNOS, Erk1/2, Akt (BD Biosciences), P-Akt, P-eNOS, or P-Erk1/2 (Cell Signaling Technology).

Recombinant cav-1 and Δrecombinant cav-1 purification. phCav-1V5 and phΔcav-1V5His plasmids were constructed as described previously (8), whereas recombinant cav-1 (rcav-1) and Δrcav-1 were purified by our modified procedure. Briefly, transfected 293PE cells were washed with PBS and lysed with 10 mL of ice-cold buffer A [50 mmol/L phosphate buffer, 300 mmol/L NaCl, 10 mmol/L imidazole, and 5 mmol/L mercaptoethanol (pH.8)] containing 0.5% Triton X-100 and 0.7% octylβ-D-glucopyranoside (OGP). The lysate was centrifuged for 15 min at 4°C, 12,000 × *g*, and the supernatant was mixed and incubated with 1 mL of Ni-NTA agarose slurry for 3 h. The resultant mixture was loaded on to a 10 mL polyprep column (Bio-Rad), and the resin was washed with 10 volumes of buffer A containing 500 mmol/L NaCl, 50 mmol/L imidazole, and 0.2% OGP. The bound cav-1-V5-His was eluted with 3 mL of elution buffer (buffer A containing 300 mmol/L imidazole, 300 mmol/L NaCl, and 0.1% OGP). For Western blot analysis, the crude supernatant as well as unbound and eluted fractions were subjected to SDS-PAGE. FITC labeling of recombinant cav-1 proteins was prepared with the EZ-label FITC

Requests for reprints: Timothy C. Thompson, The University of Texas M. D. Anderson Cancer Center, Department of Genitourinary Medical Oncology, Unit 1374, 1515 Holcombe Boulevard, Houston, TX 77030. Phone: 713-792-9955; Fax: 713-792-9956; E-mail: timthomp@mdanderson.org.

doi:10.1158/0008-5472.CAN-07-2668

protein labeling kit (Pierce Biotechnology, Inc.) according to the manufacturer's instructions.

Tubule formation assay. The *in vitro* tubule formation assay was used as described previously (12). Briefly, endothelial cells were incubated in growth factor–reduced Matrigel-coated 24-well plates in 0.5 mL of endothelial basement medium (EBM; Cambrex) in the presence or absence of rcav-1 or Δrcav-1. Images of tubule structures that formed after 18 to 24 h were captured by phase contrast microscopy, and the length of the endothelial network was quantified by image analysis of five low-power fields using free object quantification software (NucleoTech Corp.).

Wound-healing migration assay. Endothelial cells were cultured in 24-well plates to 70% to 80% confluency in EGM, and a straight longitudinal incision was made on the monolayer. After a wash with EBM and incubation with rcav-1 or Δrcav-1 in EBM containing 0.1% bovine serum albumin (BSA) for 4 h followed by an additional 48 h of incubation in EBM containing 2% of fetal bovine serum (FBS), the cells were stained with the Protocol HEMA3 stain set (Biochemical Sciences, Inc.), and the number of cells migrating into the cleared area were counted with a microscope, using advanced colony counting software (NucleoTech Corp.).

Cell proliferation and [^{3}H]-thymidine incorporation. Endothelial cells were seeded into 12-well plates (5×10^4 cells per well) and incubated overnight. After the medium was removed, the cells were treated with rcav-1 in EBM for 4 h and incubated for an additional 48 h in EBM containing 2% FBS, after which they were trypsinized and counted with a coulter counter. For [^{3}H]-thymidine uptake, the endothelial cells were seeded into 96-well plates (2.5×10^3 cells per well) in EGM then treated with rcav-1 and incubated for 48 h in EGM. [^{3}H]-thymidine (5 μCi/mL) was then added, the cells were incubated for 24 h, and the cell lysate-associated radioactivity was counted.

Nitric oxide determination. The basal and rcav-1 stimulated NO derived from endothelial cells that had accumulated in EBM over a 24-h period was measured with the Nitric Oxide Colorimetric Assay (Roche Diagnostics).

PP1 and PP2A activities. Endothelial cells were treated with rcav-1 and incubated in EBM containing 0.1% BSA for 24 h at 37°C and 5.5% CO_2. The cells were lysed with ice-cold phosphatase lysis buffer, and PP1 and PP2A activities were measured after immunoprecipitation as described previously (13).

Animal models. Orthotopic RM-9 tumors were generated by injecting 5×10^3 cells directly into the dorsolateral prostates of *cav-1*$^{+/+}$ or *cav-1*$^{-/-}$ male mice. The resultant tumors were removed at necroscopy on day 21 postinjection, and their wet weight were determined; all tumors were processed for specific immunostaining protocols (see below).

To generate the LNCaP cav-1 tet-on system, we transfected *cav-1*$^{-/-}$ low passage (LP)-LNCaP cells with pTetOn vector (Clontech), isolated stable G418-resistant clones, and screened them in a transient trasfection reporter assay with pTRE2Luc vector according to the manufacturer's protocol with or without 1 μg/mL doxycycline. Clone LNT36, which had the highest induction level, was chosen for the second cotransfection, in which a pTRECav-1 vector containing full-length human *cav-1* cDNA and the pBabeHygro plasmid were used. Double stable G418- and hygromycin-resistant clones were isolated and tested for cav-1 induction in response to the doxycycline (1.0 μg/mL). Clone LNTB25cav, which showed strong induction of cav-1 after addition of doxycycline to the medium and the lowest endogenous expression in the absence of the drug *in vitro*, was used for further *in vivo* studies.

To establish xenografts, we inoculated male nude mice with LNTB25cav cells that were suspended in Matrigel matrix and injected s.c. Tumors were present 21 days after inoculation, and tumor-bearing mice were divided into two groups that were normalized for tumor size. One group was treated with drinking water containing doxycycline (2 mg/mL) and 5% sucrose, whereas the other (control group) was treated with drinking water containing only 5% sucrose. After 21 days, the animals were sacrificed, and the tumor tissues were harvested and either snap frozen in liquid nitrogen or fixed in 10% neutral formalin.

For the *in vivo* metastasis assay, 1×10^6 LNTB25cav cells were injected into the tail veins of male nude mice to establish experimental metastases. Two months after the initial injection, the mice were divided into two groups: one was treated with drinking water containing doxycycline (2 mg/mL) and 5% sucrose and the other (control group) with drinking water containing only 5% sucrose. After a 42-day treatment, the animals were sacrificed and lung tissue was collected, fixed, and analyzed for tumor foci.

Immunohistochemistry and deconvolution microscopy. Depending on the fluorescent protein treatment, LNCaP, PC-3, and TSU-Pr1 tumor cells or endothelial cells were placed on glass coverslips in 24-well plates and incubated overnight in RPMI 1640 or EGM, respectively. After removal of the medium, the cells were washed twice with PBS buffer, then FITC-rcav-1, FITC-Δrcav-1, Alexa fluor 594–labeled cholera toxin B, and transferrin (Invitrogen) were added to medium that contained 0.1% BSA. The cells were incubated for 5 h, rinsed twice with PBS buffer, and fixed in 4% formaldehyde for 5 min at room temperature.

For immunostaining, fixed cells were permeabilized for 5 min with 0.1% Triton X-100 in PBS buffer and blocked with 3% normal horse or goat serum. They were then incubated with primary antibody followed by biotinylated anti-rabbit IgG (Vector Labs) and rhodamine-conjugated streptavidin or FITC-streptavidin (Jackson Immuno Research). Reactions were evaluated with the Delta Vision Deconvolution Microscopy System (Applied Precision, Inc.), in which a Z-series of optical sections (0.15-μm steps) were digitally imaged and deconvolved with the Delta Vision–constrained iterative algorithm to generate high-resolution images.

Mouse model–derived tumor specimens were stained for CD31 (BD Biosciences) using the avidin-biotin-peroxidase complex technique (ABC kit; Vector Lab) as previously described (14). Quantitative analysis of microvessel density was performed on the stained sections. The vascular "hot region" was first identified by low-power screening (magnification, ×40). Vascular counting was then performed on at least five 200× measuring fields (each with a real area of 0.198 mm^2). For each sample, the highest count per field was used.

Dual-immunofluorescence staining was also performed on these tissues. Briefly, after tissue sections were deparaffinized and rehydrated through graded alcohol, they were heated in 0.01 mol/L citrate buffer at pH 6.0 by microwave for 10 min to enhance antigen retrieval. After a 20-min blocking step with 1.5% normal goat serum, the sections were sequentially incubated with polyclonal cav-1 antibody diluted 1:200 for 90 min, followed by biotinylated anti-rabbit IgG and streptavidin-FITC for 30 min each. The sections were rinsed and reblocked in 1.5% normal horse serum for 20 min and incubated in CD31 rat monoclonal antibody followed by Cy-3–conjugated anti-rat IgG for 30 min. The specificity of immunoreactions was verified by replacing the primary antibodies with PBS or with corresponding normal serum. The labeled specimens were evaluated using a Zeiss fluorescence microscope equipped with a video camera (Hamamatsu). Each section was analyzed systematically, field-by-field (300×400 μm^2), over the area of cancer cells. The percentages of cav-1–positive CD31 microvessels were determined for each field for each fluorophore and on superimposed images of both fluorophores with the aid of OPTIMAS (6.0) software.

Statistical analysis. The Mann-Whitney rank test was used to analyze differences in microvessel density within mouse prostate cancer tissues; comparisons of *in vitro* tubule formation, cell migration, phosphatase activity assay, NO release assay, and RM-9 tumor wet weights relied on the unpaired two-sided *t* test. Fisher's exact test was used for the comparison of the metastasis frequency in LNTB25cav-injected mice. All statistical analyses were performed with Statview software (Version 5.0; SAS Institute).

Results

Cav-1 uptake by prostate cancer cells and endothelial cells. We have shown that prostate cancer cells secrete cav-1 possessing antiapoptotic activity that can be suppressed by cav-1–specific antiserum *in vitro* (7). Such antiserum also suppressed metastasis *in vivo*, raising the possibility that secreted cav-1 is taken up by tumor cells or tumor-associated endothelial cells or both. Thus, we treated cav-1–negative LP-LNCaP tumor cells or primary

endothelial cells, isolated from *cav-1*$^{-/-}$ mouse aorta, with conditioned medium collected from cav-1–transfected LP-LNCaP cells or with rcav-1 alone. Western blot analysis showed that cav-1 contained in conditioned medium was taken up by LP-LNCaP cells in a dose- and time-dependent manner, as indicated by the appearance of cav-1 in cell lysates within 1 h and the achievement of maximal intracellular levels 3 h posttreatment (Fig. 1*A*). Rcav-1 protein was also taken up by the LP-LNCaP cells and *cav-1*$^{-/-}$ endothelial cells in a dose-dependent fashion over a 24-h incubation period (Fig. 1*B* and *C*). Rcav-1 uptake by tumor cells (LP-LNCaP, TSU-Pr1, and PC-3) and endothelial cells [human umbilical vascular endothelial cell (HUVEC), and mouse *cav-1*$^{-/-}$ and *cav-1*$^{+/+}$] was further shown by fluorescence and deconvolution microscopy. FITC-rcav-1 uptake by these cells was temperature dependent, with 5 h of incubation at 0°C, abolishing uptake altogether (data not shown). Internalized FITC-rcav-1 was distributed throughout the cytoplasm (Fig. 1*D*).

Lipid raft/caveolae-dependent and clathrin-dependent endocytic pathways are involved in rcav-1 internalization in endothelial cells. To determine the endocytic pathways responsible for rcav-1 internalization, we pretreated HUVEC and *cav-1*$^{+/+}$ or *cav-1*$^{-/-}$ mouse endothelial cells with methyl-β-cyclodextrin (MCD) or chlorpromazine to disrupt the formation of cholesterol-rich raft microdomains or clathrin-coated pits, respectively. Fluorescence microscopy revealed that MCD effectively inhibited FITC-rcav-1 uptake in both types of endothelial cells, whereas chlorpromazine inhibited FITC-rcav-1 uptake effectively in mouse endothelial cells but only marginally in HUVEC (Fig. 2*A*). Under the same conditions, MCD effectively reduced the uptake of cholera toxin B, whereas chlorpromazine reduced the uptake of transferrin substances known to penetrate cells through cholesterol-rich lipid raft and clathrin endocytic pathways, respectively (Fig. 2*B*). These results indicate that internalization of exogenous rcav-1 proceeds through lipid raft/caveolae and clathrin pathways in both HUVEC and mouse endothelial cells, with the former pathway dominant in HUVEC (Fig. 2*A, left*). To directly show that rcav-1 associates with internalized lipid rafts/caveolae to enter endothelial cells, we incubated HUVEC for 5 h with a mixture of FITC-rcav-1 and cholera toxin B and tested for their cellular colocalization. We found that a majority (76%) of the FITC-rcav-1–positive endosomes also contained cholera toxin B (Fig. 2*C*), indicative of a requirement for caveolae and ganglioside G_{M1} lipid rafts in cav-1 penetration of human endothelial cells.

Internalization of rcav-1 is mediated by cav-1 scaffolding domain. Mutagenesis experiments have identified cav-1 scaffolding domain (CSD) residues 82 to 101 as the region responsible for mediating interactions with a number of signaling proteins including the endothelial form of nitric oxide synthase (eNOS), platelet-activating factor receptors, epidermal growth factor, the kinases Src and Fyn, heterotrimeric G protein,

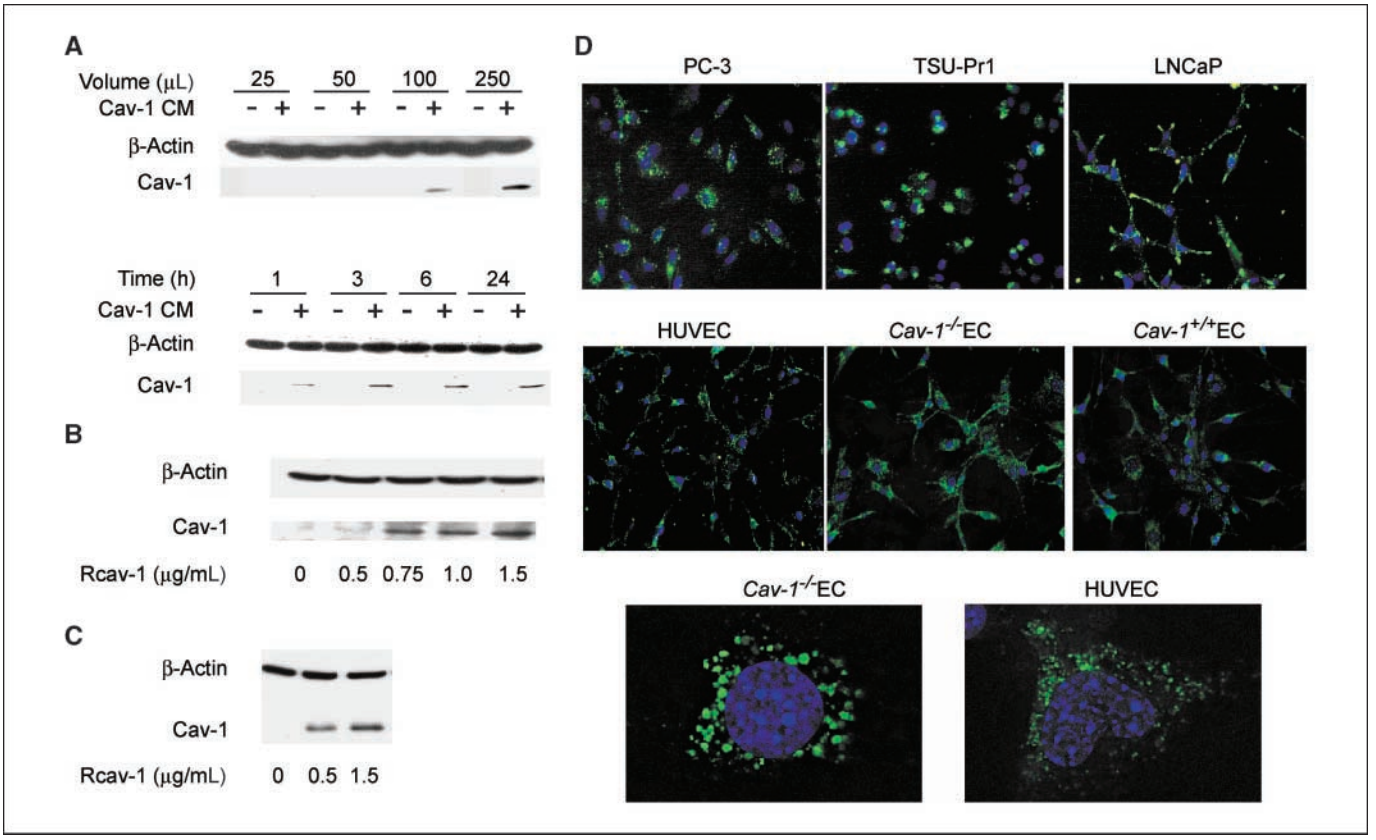

Figure 1. Cav-1 uptake by prostate cancer and bladder cancer cells and endothelial cells. *A,* dose- and time-dependent uptake of cav-1 from *cav-1*–transfected (+) or control-transfected (−) conditioned medium (*CM*) by LP-LNCaP cells. *Top,* detection of cav-1 after a 24-h treatment with conditioned medium over a range of volumes; *bottom,* detection after 1 to 24 h of treatment with 250 μL conditioned medium. *B* and *C,* dose-dependent rcav-1 uptake by LP-LNCaP tumor cells (*B*) and *cav-1*$^{-/-}$ endothelial cells (*EC*; *C*) treated for 24 h. *D,* internalization of FITC-rcav-1 by cancer cells (*top*) and endothelial cells (*middle*) treated with 3.0 μg/mL of FITC-rcav-1 for 5 h. Uptake by endothelial cells (*cav-1*$^{-/-}$ endothelial cells and HUVEC) were imaged by deconvolution microscopy after treatment with FITC-rcav-1 (*bottom*); nuclei were visualized by Hoechst 33342 staining.

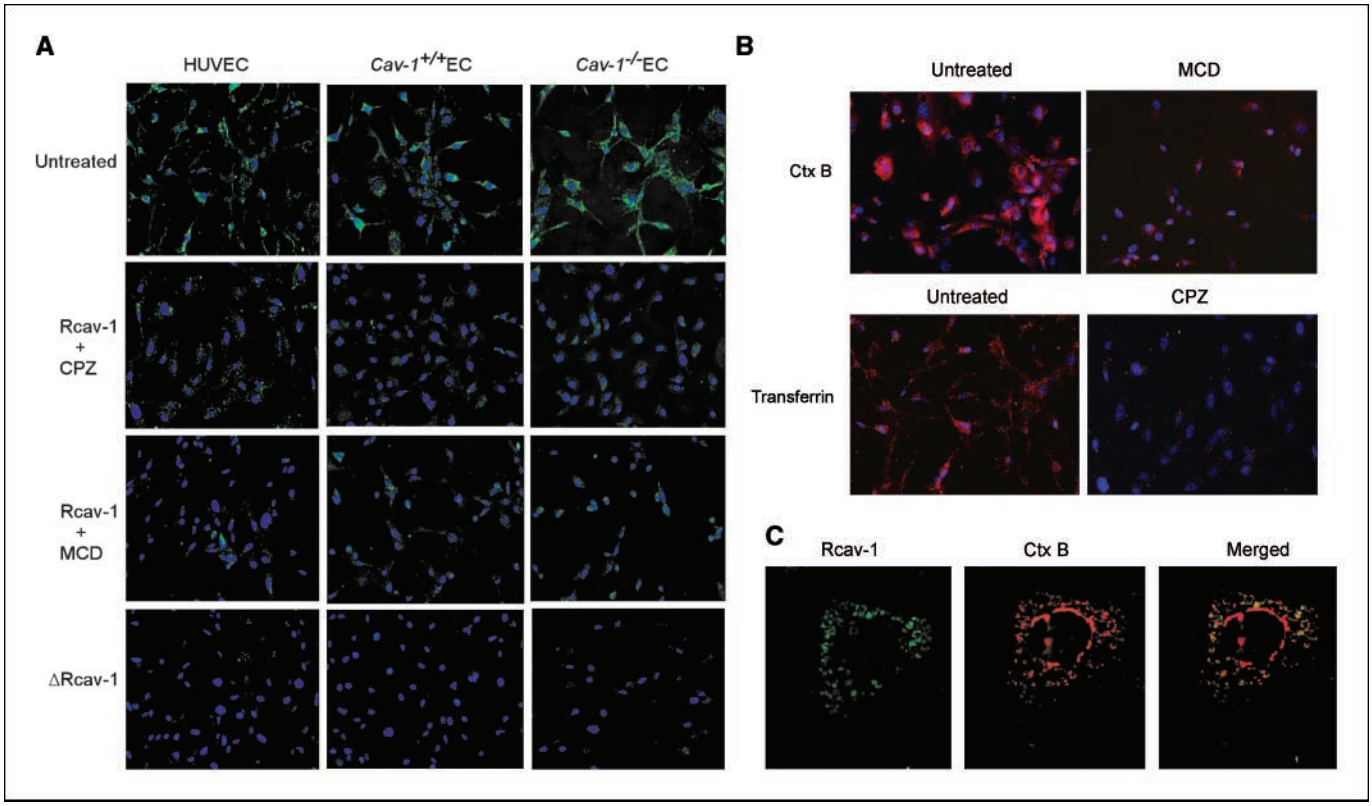

Figure 2. Internalization of rcav-1 by lipid raft/caveolae-dependent and clathrin-dependent endocytic pathways. *A,* cells were incubated with FITC-rcav-1 (3.0 μg/mL) in the presence or absence of 7.5 μg/mL of chlorpromazine (*CPZ*) or 7 mmol/L MCD for 5 h and analyzed by fluorescence microscopy. *B,* cholera toxin B (*Ctx B*) and transferrin internalization are blocked by MCD and chlorpromazine, respectively. HUVEC cells were incubated with Alexa fluor 594–labeled cholera toxin B and transferrin containing the same MCD and chlorpromazine concentrations as in *A* for 5 h and analyzed by fluorescence microscopy. Cholera toxin B internalization was impaired by cholesterol depletion (MCD treatment), whereas transferrin uptake was blocked by disruption of clathrin-coated pits (chlorpromazine treatment). *C,* colocalization of internalized FITC-rcav-1 with cholera toxin B, a ganglioside G_{M1} lipid raft/caveolae marker, as detected by deconvolution microscopy of HUVEC cells after the incubation for 5 h with FITC-rcav-1 and Alexa fluor 594–labeled cholera toxin B; nuclei were visualized by Hoechst 33342 staining.

and cholesterol-binding protein (15). This domain also targets the full-length endogenous cav-1 to lipid rafts/caveolae and cell membranes (16). To determine the role of the CSD in exogenous rcav-1 membrane attachment and cellular uptake, we generated and purified the CSD-deleted rcav-1 protein (Δrcav-1), treated endothelial cells and prostate cancer cells with different concentrations of FITC-Δrcav-1 over 1 to 6 h, and examined the cells for Δrcav-1 uptake using fluorescence microscopy. We did not detect internalized FITC-Δrcav-1 in cells incubated for as long as 6 h at concentrations of the mutant protein ranging to 5.0 μg/mL (Fig. 2*A*). In separate coincubation experiments, we showed uptake of cholera toxin B or transferrin under the same conditions (data not shown). These observations suggest that endocytosis of exogenous rcav-1 protein and its subsequent stimulation of angiogenic activities is mediated, in part, by CSD, which seems critical for cellular internalization of the protein.

Rcav-1 stimulates differentiation and migration of *cav-1*$^{-/-}$ endothelial cells. We initially analyzed the formation of tubules by endothelial cells, isolated from *cav-1*$^{+/+}$ or *cav-1*$^{-/-}$ aorta, on growth factor–reduced Matrigel. Compared with *cav-1*$^{+/+}$ endothelial cells, cells lacking this gene showed significantly reduced tubule formation in the absence of rcav-1 stimulation (Fig. 3*A*; micrographs). However, treatment with rcav-1 stimulated tubule formation in *cav-1*$^{-/-}$ endothelial cells in a dose-dependent manner with a >2-fold increase in tubule length observed with use of 1.5 μg/mL rcav-1 compared with untreated controls (P = 0.021). Importantly, Δrcav-1 at this concentration failed to stimulate tubule formation (Fig. 3*A*). To determine the effects of rcav-1 on *cav-1*$^{-/-}$ endothelial cell migration, we used the *in vitro* wound-healing assay. Rcav-1 treatment stimulated *cav-1*$^{-/-}$ endothelial cell migration in a dose-dependent fashion with a 2-fold increase in the number of migratory cells at a rcav-1 concentration of 1.5 μg/mL (P = 0.019), whereas Δrcav-1 at this concentration failed to increase migration/motility of the endothelial cells (Fig. 3*B*). This enhancement of tubule formation and the number of migratory/motile cells by rcav-1 treatment did not result from increased cell proliferation, as the numbers of cells or levels of thymidine uptake posttreatment were similar to the results for untreated controls (data not shown).

Rcav-1 stimulates the angiogenic activities in *cav-1*$^{-/-}$ endothelial cells through the activation of eNOS. Caveolae and cav-1 play critical roles in ensuring the coupling between vascular endothelial growth factor (VEGF) receptors and downstream mediators of angiogenesis, such as VEGF, which activates Erk and eNOS via the phosphatidylinositol-3-kinase (PI3-K)-Akt signaling pathway (17–19). Thus, to assess the contribution of this signaling module to the angiogenic activities of rcav-1, we tested the effects of inhibitors of PI3 kinase (LY294002), eNOS (L-NAME), and Erk (PD98059) in *cav-1*$^{-/-}$ endothelial cells. Figure 3*C* and *D* shows that both LY294002 and L-NAME, but not PD98059, significantly suppressed rcav-1–stimulated angiogenesis, implicating PI3-K-Akt-eNOS signaling in the pathologic angiogenic effects

of cav-1 in prostate cancer cells. To investigate this possibility further, we measured the levels of accumulated NO (NO_2^- + NO_3^-) at 24 h after rcav-1 treatment of *cav-1*$^{-/-}$ endothelial cells. NO release by these cells was significantly increased by rcav-1 in a dose-dependent manner (P = 0.029 versus untreated control; Fig. 4*A, left*). Analysis of the effects of rcav-1 on the phosphorylation status of Akt and its downstream target protein eNOS in *cav-1*$^{-/-}$ endothelial cells showed a dose-dependent increase in Akt phosphorylation on S473 and T308 with no change in total Akt. Rcav-1 treatment also led to increased eNOS phosphorylation on S1177 but not T495 (Fig. 4*A, right*). The CSD-deleted rcav-1 failed to stimulate eNOS S1177 phosphorylation, as expected (Fig. 4*B, top*). We also tested the effect of LY294002 on the rcav-1–induced phosphorylation of Akt (T308) and eNOS (S1177) in *cav-1*$^{-/-}$ endothelial cells. As expected, LY294002 treatment of the cells diminished the observed Akt phosphorylation induction by rcav-1. Interestingly, the phosphorylation of eNOS (S1177) induced by rcav-1 was reduced but not completely diminished as a result of LY294002 treatment (Fig. 4*B, bottom*).

To further investigate the mechanism(s) that underlies rcav-1–stimulated eNOS activation, we tested the effect of rcav-1 on the activities of serine/threonine protein phosphatases PP1 and PP2A in *cav-1*$^{-/-}$ endothelial cells. These two phosphatases are known to regulate the phosphorylation of multiple protein targets including Akt and eNOS (20, 21) and are inhibited by cav-1 overexpression in prostate cancer cells (13). The activation of eNOS by a number of stimuli including VEGF involves a transient increase in the phosphorylation of S1177 with a decrease in T495 phosphorylation, alternatively, protein kinase C signaling inhibits eNOS activity by phosphorylating T495 and dephosphorylating S1177. Both PP1 and PP2A are associated with eNOS phosphorylation. PP1 is specific for dephosphorylation of T495, whereas PP2A is specific for S1177

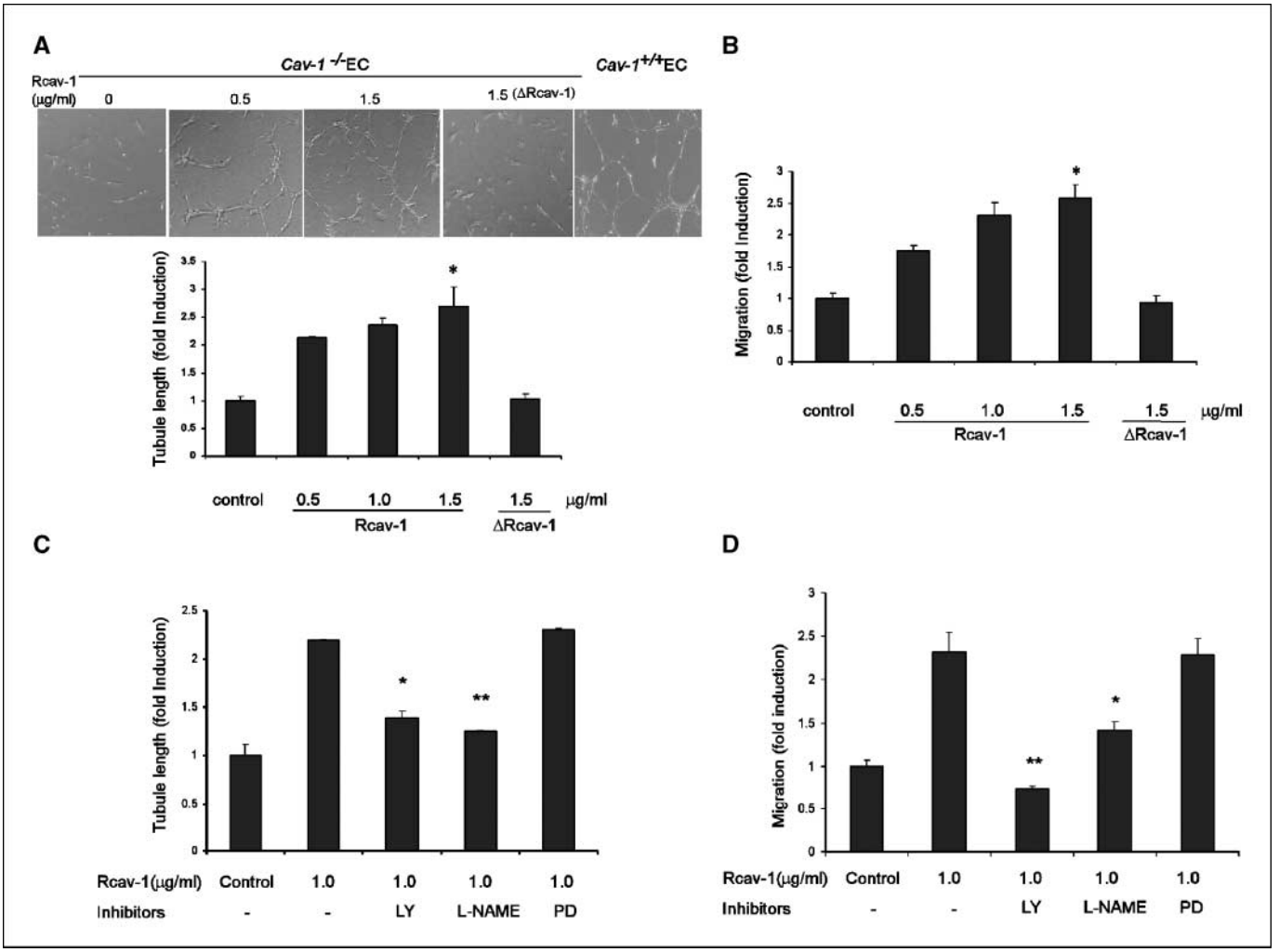

Figure 3. Rcav-1 stimulates tubule formation and cell migration in *cav-1*$^{-/-}$ endothelial cells. *A,* representative micrographs showing newly formed tubules of *cav-1*$^{+/+}$ and *cav-1*$^{-/-}$ endothelial cells cultured on growth factor–reduced Matrigel under basal conditions or after treatment with 0.5 to 1.5 μg/mL of rcav-1 and 1.5 μg/mL Δrcav-1 for 18 h. Bar graph depicts dose-dependent rcav-1 or Δrcav-1 stimulation of tubule formation in *cav-1*$^{-/-}$ endothelial cells. The values are folds of induction relative to untreated control ± SD of three independent experiments. *, P = 0.02 versus untreated control by two-sided t test. *B,* dose-dependent rcav-1 or Δrcav-1 stimulation of *cav-1*$^{-/-}$ endothelial cell migration in a wound-healing assay. The values are folds of induction relative to untreated control ± SD of three independent experiments. *, P = 0.0193 versus untreated control by two-sided t test. *C,* inhibition of rcav-1–stimulated tubule formation by LY294002 (*LY*; 3.0 μmol/L) or L-NAME (1.0 mmol/L) but not by PD98059 (*PD*; 50 μmol/L) in *cav-1*$^{-/-}$ endothelial cells. *, P = 0.008; **, P = 0.003 versus rcav-1 treated only. *D,* inhibition of rcav-1–stimulated wound-healing assay cell migration by LY294002 (3.0 μmol/L) or L-NAME (1.0 mmol/L), but not by PD98059 (50 μmol/L) in *cav-1*$^{-/-}$ endothelial cells. *, P = 0.011; **, P = 0.005 versus rcav-1 treated only, by-two sided t test. Bar graphs in *C* and *D* represent tubule length relative to untreated controls and the number of migratory cells relative to untreated controls, respectively. *Columns,* mean; *bars,* SD.

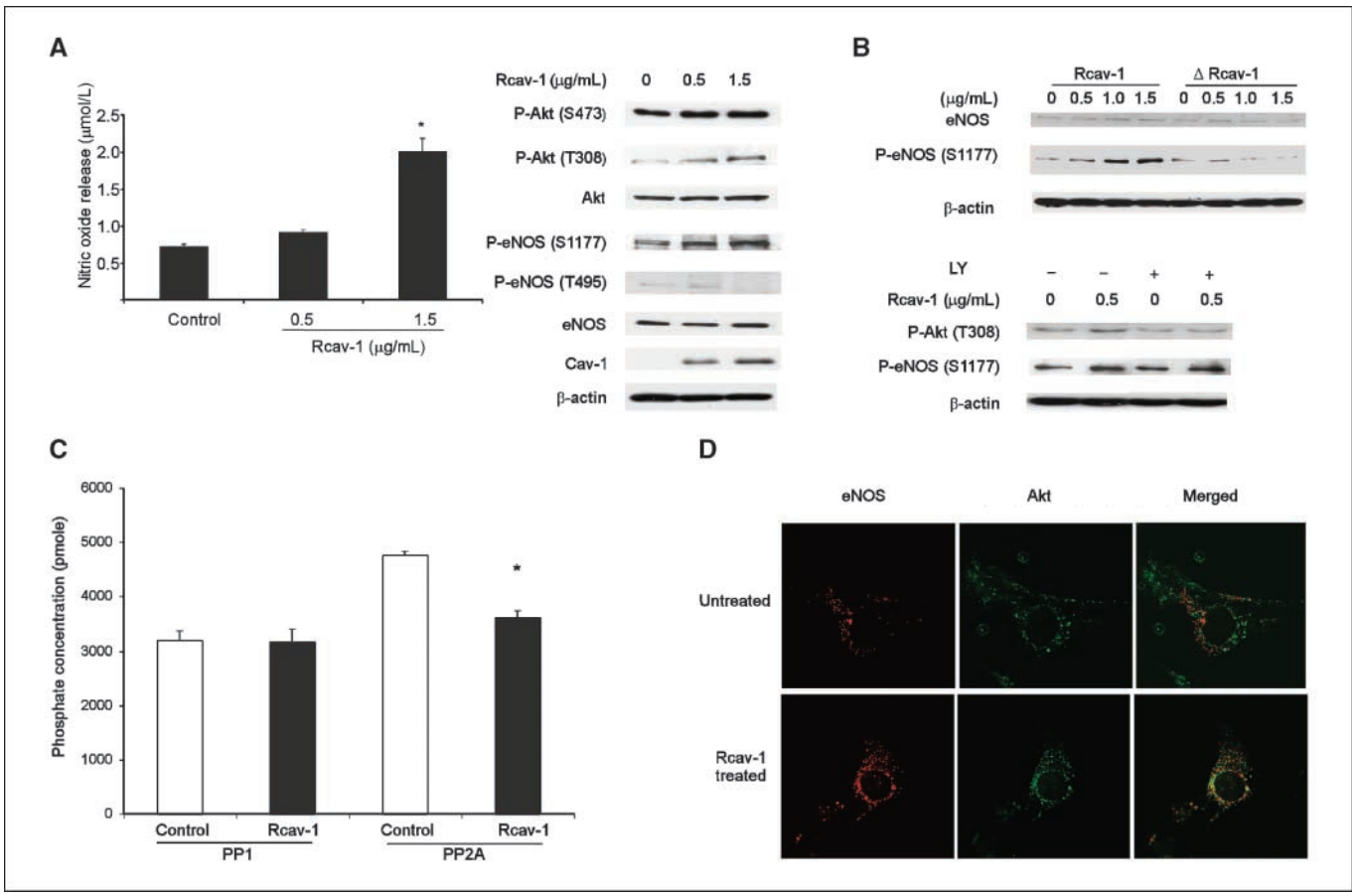

Figure 4. Rcav-1 is involved in PI3-K-Akt-eNOS–mediated stimulation of angiogenic activities in *cav-1*$^{-/-}$ endothelial cells. *A,* dose-dependent NO release by *cav-1*$^{-/-}$ endothelial cells after rcav-1 treatment. *Columns,* mean; *bars,* SD. *, $P = 0.029$ versus untreated control, by two-sided *t* test (*left*). Increased phosphorylation of Akt on S473 and T308, and of eNOS on S1177 by Western blot analysis of *cav-1*$^{-/-}$ endothelial cells lysates treated for 24 h with different concentrations of rcav-1 (*right*). *B,* Δrcav-1 treatment of *cav-1*$^{-/-}$ endothelial cells for 24 h does not affect the phosphorylation status of eNOS on S1177, but rcav-1 increases eNOS phosphorylation on S1177 in a dose-dependent fashion (*top*). Treatment of *cav-1*$^{-/-}$ endothelial cells with LY29400 abolishes the rcav-1–induced Akt phosphorylation on T308 and reduces, but does not completely eliminate, the eNOS phosphorylation on S1177 induced by rcav-1 (*bottom*). *C,* rcav-1 inhibits the activity of PP2A but not PP1 in *cav-1*$^{-/-}$ endothelial cells. PP1-C or PP2A-C immunprecipitation complexes from rcav-1–treated *cav-1*$^{-/-}$ endothelial cells or untreated controls were used to determine phosphatase activities with the serine/threonine protein phosphatase assay. *Columns,* mean; *bars,* SD. *, $P = 0.0002$ by two-sided *t* test. *D*, induction of eNOS/Akt association by rcav-1. *Cav-1*$^{-/-}$ endothelial cells were cultured for 6 h in the presence or absence of rcav-1. After fixation, the cells were double-labeled with anti-eNOS and anti-Akt immunofluorecence. In untreated cells, eNOS (*red*) and Akt (*green*) were localized to separate compartments (*top*), whereas rcav-1 protein treatment of the cells for 6 h induced eNOS (*red*) and Akt (*green*) colocalization in cytoplasmic vesicles (*bottom*), as visualized by deconvolution microscopy.

dephosphorylation (21). The results showed that rcav-1 treatment significantly inhibited the activity of PP2A but had no effect on PP1 activity ($P = 0.0002$ versus control; Fig. 4*C*). These data provide evidence that rcav-1 induces eNOS phosphorylation through Akt activation, and independently of Akt, through inhibition of PP2A, which specifically dephosphorylates eNOS (S1177).

A number of studies have shown that both eNOS and PI3 kinase are colocalized within the caveolar region of the plasma membrane (22, 23); therefore, we investigated the role played by cav-1 in compartmentalization of the PI3-K-Akt-eNOS signaling pathway molecules in *cav-1*$^{-/-}$ endothelial cells. We incubated the cells with or without rcav-1 for 5 h and visualized the cells by deconvolution microscopy for colocalization of Akt with eNOS. We found that Akt was not colocalized with eNOS in untreated cells, whereas significant colocalization of the two molecules was observed in the cells treated with rcav-1 (Fig. 4*D*).

Rcav-1 uptake in tumor-associated endothelial cells and proangiogenic activities in prostate cancer animal models. To investigate the effects of endothelial cells–localized cav-1 on microvessel density and tumor growth *in vivo*, we used an orthotopic RM-9 mouse prostate cancer model (24), in which cav-1 expressing and secreting RM-9 prostate cancer cells are injected directly into the dorsolateral prostate of male *cav-1*$^{+/+}$ or *cav-1*$^{-/-}$ mice. In this model, the mean (1.85 ± 0.167) tumor wet weight was significantly higher in *cav-1*$^{+/+}$ versus *cav-1*$^{-/-}$ mice ($P = 0.045$; Fig. 5*A*). Moreover, immunohistochemical analysis of tumor sections collected from sacrificed mice showed that RM-9 tumors had significantly higher microvessel densities in *cav-1*$^{+/+}$ compared with *cav-1*$^{-/-}$ hosts [median, 21.5 (range, 15.6–36.1) versus 13.3 (range, 8.2–22.8; $P = 0.0078$); Fig. 5*B* and *C*]. Interestingly, >70% of the CD31^{+} microvessels in the *cav-1*$^{-/-}$ mouse tumor sections were positive for cav-1 staining, indicating uptake of RM-9 cell–derived cav-1 by tumor-associated endothelial cells (Fig. 5*D, arrows*).

We examined the association between cav-1 expression and prostate tumor–associated angiogenesis more closely by generating an LNCaP tet-on cav-1 stable cell line (LNTB25cav) in which the expression of cav-1 can be regulated by manipulating doxycycline. In the absence of doxycycline, the level of cav-1 protein in lysate is low, whereas the addition of doxycycline to the culture medium

leads to a rapid induction of cav-1 protein *in vitro* (Fig. 6*A*). LNTB25cav tumors were established as s.c. growing xenografts in adult male nude mice; tumor-bearing mice were then treated with either doxycycline or control sucrose solution added to the drinking water. Tumor volumes in the doxycycline-treated group were significantly greater than those in the control group on days 12, 15, and 18 after treatment ($P = 0.0195$, $P = 0.035$, $P = 0.019$, respectively; Fig. 6*A*). Further immunohistochemical analysis showed increased cav-1 levels in the cytoplasm of tumor cells in doxycycline-treated compared with control mice (Fig. 6*B, top*). Microvessel densities determined by CD31 labeling were greater in cav-1–induced tumors compared with controls ($P = 0.039$; Fig. 6*B, bottom*; Fig. 6*C*). In separate experiments, we injected 1×10^6 LNTB25cav cells into the tail veins of nude mice to establish experimental lung metastases. After 42 days of continuous treatment, the number and frequency of lung metastases in doxycycline-treated animals significantly exceeded results in the control group ($P = 0.008$ and 0.04, respectively; Fig. 6*D*) and their average size was clearly larger in doxycycline-treated mice (data not shown).

Discussion

The establishment of prostate cancer metastases involves the successful negotiation of multiple endogenous physiologic barriers, survival during transit through the blood or lymphatic stream, and colonization at distant sites. The growth and metastasis of prostate cancer and other tumors is dependent on the induction of new blood vessels from preexisting ones through angiogenesis (25, 26). Cav-1 has been implicated in the regulation of endothelial cells proliferation, differentiation, and stabilization (6, 17, 27, 28). In a study using Lewis lung carcinoma cells animal cancer model, cav-1 was found to be antiangiogenic factor (29). In contrast, the results of a number of studies including this report have shown a proangiogenic function for cav-1. In an experimental melanoma model, impairment of pathologic angiogenesis was reported in *cav-1*$^{-/-}$ compared with *cav-1*$^{+/+}$ (30). Increased expression of cav-1 and microvessel density was found to be associated with metastasis and a worse prognosis in human clear cell renal cell carcinoma, suggesting a proangiogenic role for cav-1 (31). We also presented correlative evidence for a proangiogenic role of cav-1 in human prostate cancer (4). Endogenous levels of cav-1 expression in endothelial cells may provide an explanation for this controversy. C*av-1*$^{-/-}$ endothelial cells showed abrogated tubule formation and reduced NO production with or without VEGF treatment. Enforced expression of relatively low levels of cav-1 in cav-1$^{-/-}$ endothelial cells produced increased eNOS phosphorylation (S1177) and NO production in response to VEGF treatment, yet expression of higher levels of cav-1 blocked this process (17).

Apparently, without cav-1, endothelial cells do not undergo proper maturation and maintain a hyperproliferative state. This

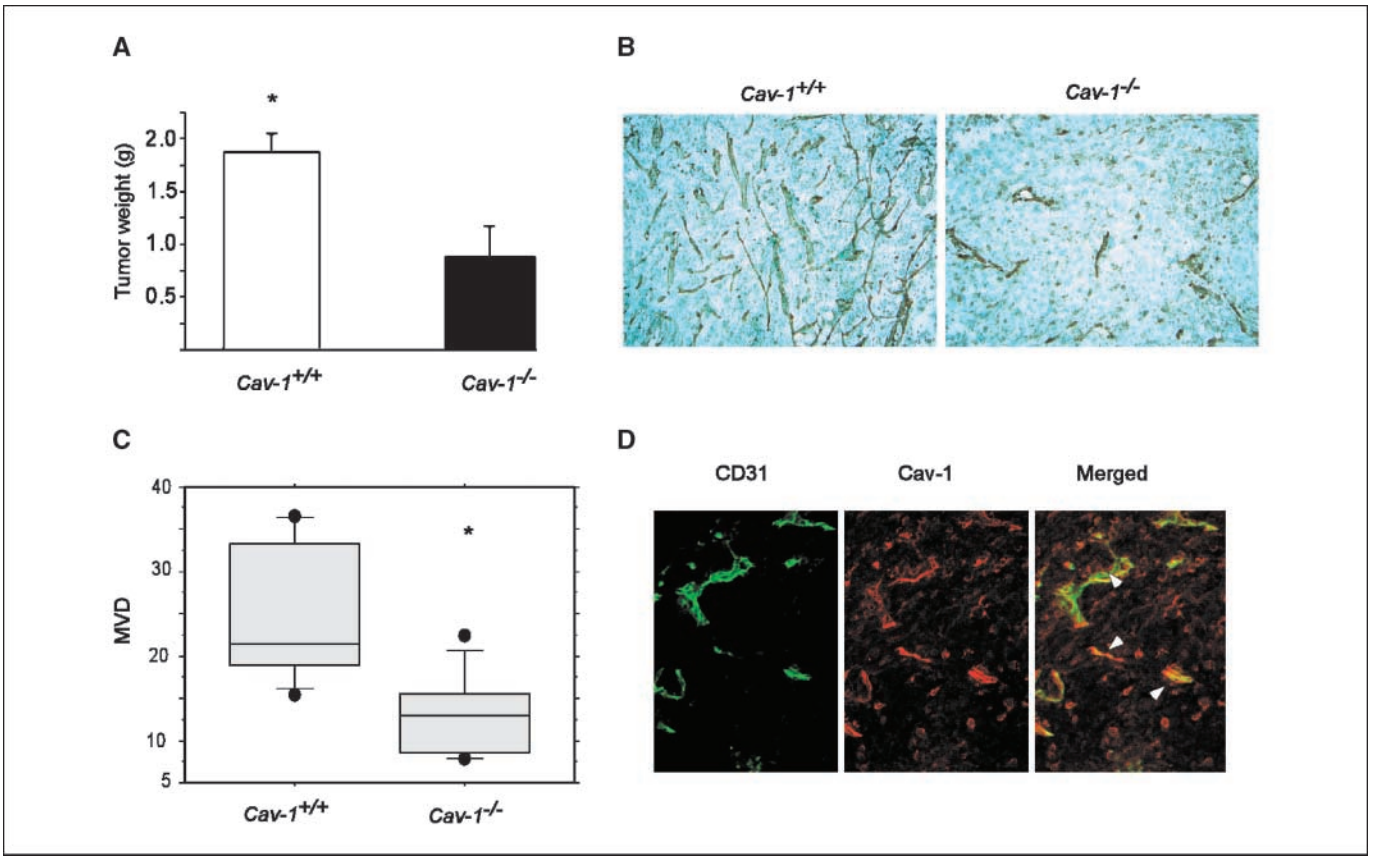

Figure 5. Secreted cav-1 promotes growth and angiogenesis in orthotopic RM-9 mouse prostate cancer model. *A,* increased RM-9 tumor wet weight in *cav-1*$^{+/+}$ hosts ($n = 7$) compared with *cav-1*$^{-/-}$ hosts ($n = 7$). *Columns,* mean; *bars,* SE. *, $P = 0.045$ by two-sided *t* test. *B,* immunohistochemical staining for CD31 in RM-9 tumors shows increased microvessel density in *cav-1*$^{+/+}$ hosts compared with *cav-1*$^{-/-}$ hosts. *C,* quantitative box plot analysis of the microvessel density (*MVD*) in RM-9 tumors from *cav-1*$^{+/+}$ versus *cav-1*$^{-/-}$ hosts. *Top lines,* 10th percentile; *bottom lines,* 90th percentile; *middle lines,* median value. *, $P = 0.0078$ by Mann-Whitney rank test. *D,* images of double immunostaining for CD31 (*green*) and cav-1 (*red*) in a tissue section of an RM-9 tumor from a *cav-1*$^{-/-}$ host. Arrows in the merged image (*yellow*) indicate the uptake by microvessels of cav-1 secreted by RM-9 tumors.

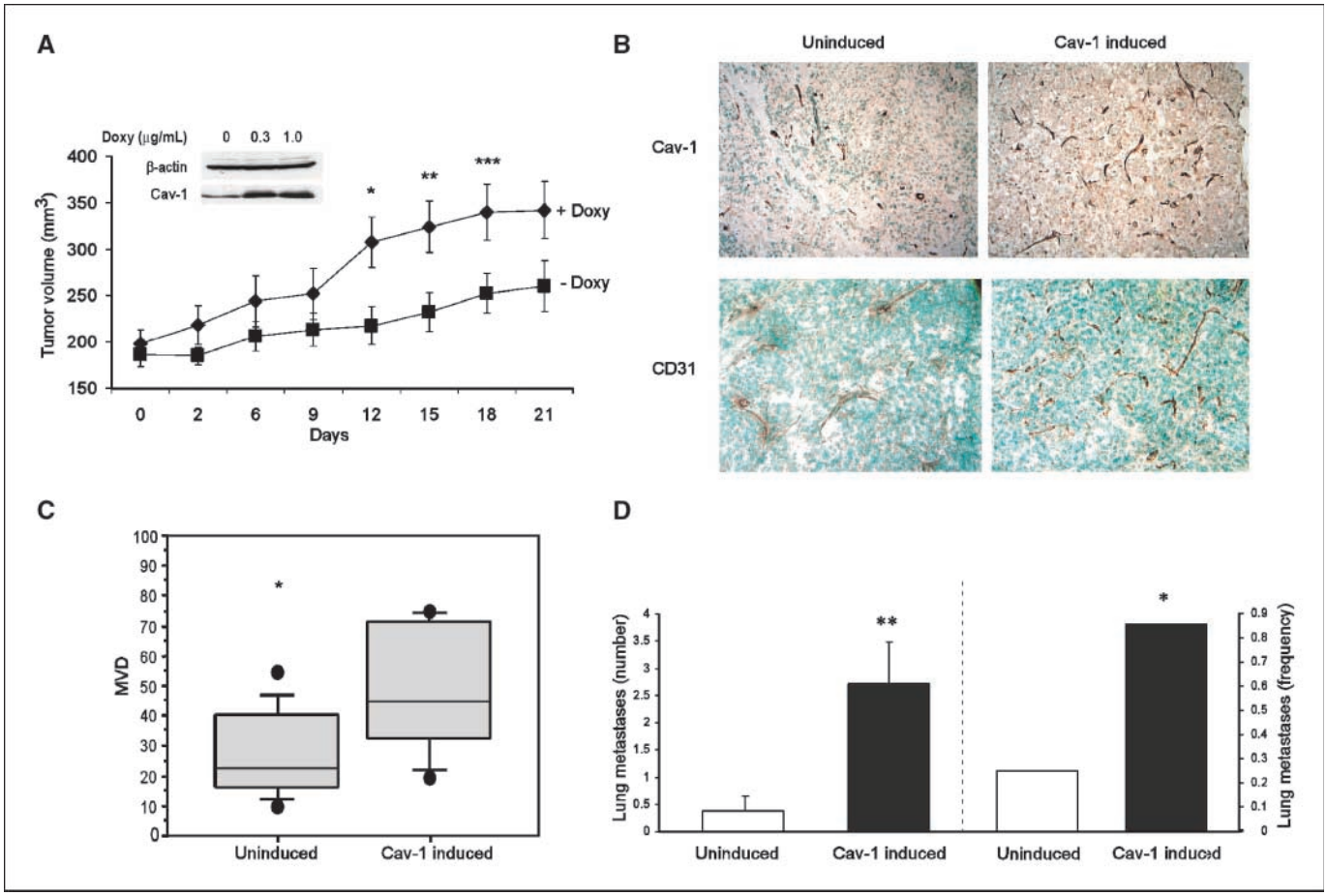

Figure 6. Secreted cav-1 promotes growth and angiogenesis in LNTB25cav tumors. *A,* Cav-1 induction by doxycycline (*Doxy*) leads to increased tumor volume in LNTB25cav s.c xenograft tumors growing s.c. Two groups of mice (n = 8 each) normalized for tumor volume were treated with either doxycycline (2 mg/mL) or control sucrose in drinking water for 21 d. *Points,* mean; *bars,* SE. *, P = 0.0195; **, P = 0.035; ***, P = 0.019 by two-sided t test. *B,* representative immunohistochemical staining for cav-1 and CD31 shows increased cytoplasmic cav-1 in cancer cells (*top*), and increased numbers of microvessels (*bottom*) in cav-1–induced LNTB25cav tumors compared with uninduced LNTB25cav tumors. *C,* quantitative box plot analysis of microvessel density in cav-1–induced (n = 8) and uninduced (n = 11) tumors. *Top lines,* 10th percentile; *bottom lines,* 90th percentiles; *middle lines,* median value. *, P = 0.039 by Mann-Whitney rank test. *D,* increased number and frequency of lung metastases in cav-1–induced compared with uninduced tumors. Lung metastases were established by injecting LNTB25cav cells into the tail veins of nude mice that were subsequently treated with doxycycline (n = 7) or sucrose (n = 8) in drinking water for 42 d. *Columns,* mean; *bars,* SE. *, P = 0.040 by Fisher's exact test; **, P = 0.008 by two-sided t test.

leads to a lack of polarization and a failure to form intercellular junctions (32), which may compromise selective transport mechanisms for specific macromolecules. Similarly, in tumor-associated endothelial cells a certain basal level of cav-1 may be required for minimal functional capacity. We have recently shown that cav-1 low/negative endothelial cells are relevant to prostate cancer. We reported significant reduction in the density of cav-1 positive microvessels in cav-1–negative human prostate cancer tissue compared with benign prostate tissues, clarifying the existence and possible significance of cav-1–negative microvessels in these malignancies (4).

We show that endocytosis of extracellular rcav-1 occurs in cancer cells (TSU-Pr1, DU145, and PC-3) and endothelial cells (HUVEC, *cav-1*$^{-/-}$ endothelial cells, and *cav-1*$^{+/+}$ endothelial cells), and that endothelial cells take up rcav-1 through lipid rafts/caveolae and clathrin-dependent pathways. Our results also show that rcav-1 uptake does not have an absolute cellular requirement for caveolae. The involvement of multiple endocytic pathways is not unique to cav-1 internalization, as these mechanisms have been described for the internalization of a number of proteins such as protein-specific membrane antigen (33), insulin growth factor binding protein-3 (34), transforming growth factor β receptor (35), and decorin (36). A possible explanation for the internalization of cav-1 through multiple pathways is its ability to interact with and bind to a large number of signaling proteins including multiple membrane receptors (15), which places it in proximity to endosome-forming activities of various pathways.

We show that CSD is necessary but may not be sufficient for cav-1 uptake, which leads to tubule formation, cell migration, and NO production in *cav-1*$^{-/-}$ endothelial cells. These data are supported by the results of a study that identified a highly conserved region of the engrailed homeoproteins that bears a high degree of homology with the CSD and are responsible for oligopeptide or oligonucleotide transmembrane, and cellular transport (37). The CSD was also found to have the ability to direct endogeneous cav-1 to cell membranes (16).

We show that cav-1 angiogenic activities involve the PI3-K-Akt-eNOS pathway but not Erk1/2. Indeed, rcav-1 treatment increases phosphorylation of Akt (S473 and T308) and, hence, eNOS phosphorylation (S1177 but not T495), leading to NO production.

Because previous studies show that Akt phosphorylates eNOS on the S1177 site, leading to eNOS activation, our results are consistent with a straight forward molecular pathway through which cav-1 uptake activates Akt, which in turn activates eNOS. However, Akt inhibitor studies indicated that Akt signaling is not the only pathway culminating in eNOS phosphorylation on S1177. That is, rcav-1–stimulated Akt activation was accompanied by inhibition of PP2A, a specific serine/threonine kinase that dephosphorylates S473 and T308 on Akt, and S1177 and T495 on eNOS (13, 21, 38). It is of interest that rcav-1 did not inhibit PP1, a serine/threonine kinase whose substrate specificity is similar to that of PP2A. Because PP1 may have selective activity for the T495 site on eNOS, which unlike the S1177 site leads to inhibition of eNOS activity, the absence of cav-1–mediated inhibition of PP1 could further contribute to eNOS activation (21). This notion is supported by the absence of increased phosphorylation of T495 on eNOS in response to rcav-1 (Fig. 4*A, right*). Because we previously showed that cav-1–stimulated PP1, and PP2A inhibition is mediated through direct interaction between the cav-1 CSD and PP1/PP2A binding sites in prostate cancer cells, (13) it seems reasonable to suggest that this specific interaction also applies to rcav-1–mediated inhibition of PP2A in *cav-1*$^{-/-}$ endothelial cells.

Studies with two complementary animal model systems (i.e., the RM-9-*cav-1*$^{-/-}$ host orthotopic model and the LNTB25cav xenograft model) substantiate our *in vitro* findings that tumor-associated endothelial cells internalize tumor-secreted cav-1, which is associated with tumor growth, and that overexpression of cav-1 in prostate cancer cells promotes angiogenesis and tumor growth.

Overall, our data show that prostate cancer cell–derived and prostate cancer cell–secreted cav-1 has autocrine (tumor cell uptake) and paracrine (tumor-associated endothelial cells uptake) activities that can contribute to angiogenesis, tumor progression, and metastasis. We propose that prostate cancer and potentially other malignancies that overexpress and secrete cav-1, may benefit from anti–cav-1 therapy that could involve cav-1 antibodies or peptide inhibitors of CSD.

Acknowledgments

Received 7/13/2007; revised 9/27/2007; accepted 11/12/2007.

Grant support: NIH grants RO1 CA68814 and Specialized Programs of Research Excellence P50 58204 and DAMD PC051247 from the Department of Defense.

The costs of publication of this article were defrayed in part by the payment of page charges. This article must therefore be hereby marked *advertisement* in accordance with 18 U.S.C. Section 1734 solely to indicate this fact.

References

1. Shaul PW, Anderson RG. Role of plasmalemmal caveolae in signal transduction. Am J Physiol 1998;275:L843–51.
2. Nasu Y, Timme TL, Yang G, et al. Suppression of caveolin expression induces androgen sensitivity in metastatic androgen-insensitive mouse prostate cancer cells. Nat Med 1998;4:1062–4.
3. Yang G, Truong LD, Timme TL, et al. Elevated expression of caveolin is associated with prostate and breast cancer. Clin Cancer Res 1998;4:1873–80.
4. Yang G, Addai J, Ayala G, et al. Correlative evidence that prostate cancer cell-derived caveolin-1 mediated angiogenesis. Hum Pathol 2007;38:1688–95.
5. Williams TM, Lisanti MP. The Caveolin genes: from cell biology to medicine. Ann Med 2004;36:584–95.
6. Carver LA, Schnitzer JE. Caveolae: mining little caves for new cancer targets. Nat Rev Cancer 2003;3:571–81.
7. Tahir SA, Yang G, Ebara S, et al. Secreted caveolin-1 stimulates cell survival/clonal growth and contributes to metastasis in androgen-insensitive prostate cancer. Cancer Res 2001;61:3882–5.
8. Tahir SA, Ren C, Timme TL, et al. Development of an immunoassay for serum caveolin-1: a novel biomarker for prostate cancer. Clin Cancer Res 2003;9:3653–9.
9. Tahir SA, Frolov A, Hayes TG, et al. Preoperative serum caveolin-1 as a prognostic marker for recurrence in a radical prostatectomy cohort. Clin Cancer Res 2006;12:4872–5.
10. Williams TM, Hassan GS, Li J, et al. Caveolin-1 promotes tumor progression in an autochthonous mouse model of prostate cancer: genetic ablation of Cav-1 delays advanced prostate tumor development in TRAMP mice. J Biol Chem 2005;10:1074.
11. Cao G, Yang G, Timme TL, et al. Disruption of the caveolin-1 gene impairs renal calcium reabsorption and leads to hypercalciuria and urolithiasis. Am J Pathol 2003;162:1241–8.
12. Brouet A, Sonveaux P, Dessy C, et al. Hsp90 and caveolin are key targets for the proangiogenic nitric oxide-mediated effects of statins. Circ Res 2001;89:866–73.
13. Li L, Ren CH, Tahir SA, Thompson TC. Caveolin-1 maintains activated Akt in prostate cancer cells through scaffolding domain binding site interactions with and inhibition of serine/threonine protein phosphatases PP1 and PP2A. Mol Cell Biol 2003;23:9389–404.
14. Vermeulen PB, Gasparini G, Fox SB, et al. Second international consensus on the methodology and criteria of evaluation of angiogenesis quantification in solid human tumours. Eur J Cancer 2002;38:1564–79.
15. Smart EJ, Graf GA, McNiven MA, et al. Caveolins, liquid-ordered domains, and signal transduction. Mol Cell Biol 1999;19:7289–304.
16. Schlegel A, Lisanti MP. A molecular dissection of caveolin-1 membrane attachment and oligomerization. Two separate regions of the caveolin-1 C-terminal domain mediate membrane binding and oligomer/oligomer interactions *in vivo*. J Biol Chem 2000;275:21605–17.
17. Sonveaux P, Martinive P, DeWever J, et al. Caveolin-1 expression is critical for vascular endothelial growth factor-induced ischemic hindlimb collateralization and nitric oxide-mediated angiogenesis. Circ Res 2004;95:154–61.
18. Labrecque L, Royal I, Surprenant DS, et al. Regulation of vascular endothelial growth factor receptor-2 activity by caveolin-1 and plasma membrane cholesterol. Mol Biol Cell 2003;14:334–47.
19. Liu J, Wang XB, Park DS, Lisanti MP. Caveolin-1 expression enhances endothelial capillary tubule formation. J Biol Chem 2002;277:10661–8.
20. Cohen PT. Protein phosphatase 1-targeted in many directions. J Cell Sci 2002;115:241–56.
21. Michell BJ, Chen Z, Tiganis T, et al. Coordinated control of endothelial nitric-oxide synthase phosphorylation by protein kinase C and the cAMP-dependent protein kinase. J Biol Chem 2001;276:17625–8.
22. Chambliss KL, Shaul PW. Rapid activation of endothelial NO synthase by estrogen: evidence for a steroid receptor fast-action complex (SRFC) in caveolae. Steroids 2002;67:413–9.
23. Stirone C, Boroujerdi A, Duckles SP, Krause DN. Estrogen receptor activation of phosphoinositide-3 kinase, akt, and nitric oxide signaling in cerebral blood vessels: rapid and long-term effects. Mol Pharmacol 2005;67:105–13.
24. Nasu Y, Bangma C, Hull G, et al. Combination gene therapy with adenoviral vector-mediated HSV-tk+GCV and IL-12 in an orthotopic mouse model for prostate cancer. Prostate Cancer Prostatic Diseases 2001;4:44–55.
25. Hanahan D, Folkman J. Patterns and emerging mechanisms of the angiogenic switch during tumorigenesis. Cell 1996;86:353–64.
26. Carmeliet P, Jain RK. Angiogenesis in cancer and other diseases. Nature 2000;407:249–57.
27. Frank PG, Woodman SE, Park DS, Lisanti MP. Caveolin, caveolae, and endothelial cell function. Arterioscler Thromb Vasc Biol 2003;23:1161–8.
28. Massimino ML, Griffoni C, Spisni E, Toni M, Tomasi V. Involvement of caveolae and caveolae-like domains in signalling, cell survival and angiogenesis. Cell Signal 2002;14:93–8.
29. Lin MI, Yu J, Murata T, Sessa WC. Caveolin-1-deficient mice have increased tumor microvascular permeability, angiogenesis, and growth. Cancer Res 2007;67:2849–56.
30. Woodman SE, Ashton AW, Schubert W, et al. Caveolin-1 knockout mice show an impaired angiogenic response to exogenous stimuli. Am J Pathol 2003;162:2059–68.
31. Joo HJ, Oh DK, Kim YS, Lee KB, Kim SJ. Increased expression of caveolin-1 and microvessel density correlates with metastasis and poor prognosis in clear cell renal cell carcinoma. BJU Int 2004;93:291–6.
32. Razani B, Engelman JA, Wang XB, et al. Caveolin-1 null mice are viable but show evidence of hyperproliferative and vascular abnormalities. J Biol Chem 2001;276:38121–38.
33. Anilkumar G, Barwe SP, Christiansen JJ, et al. Association of prostate-specific membrane antigen with caveolin-1 and its caveolae-dependent internalization in microvascular endothelial cells: implications for targeting to tumor vasculature. Microvasc Res 2006;72:54–61.
34. Lee KW, Liu B, Ma L, et al. Cellular internalization of insulin-like growth factor binding protein-3: distinct endocytic pathways facilitate re-uptake and nuclear localization. J Biol Chem 2004;279:469–76.
35. Di Guglielmo GM, Le Roy C, Goodfellow AF, Wrana JL. Distinct endocytic pathways regulate TGF-β receptor signalling and turnover. Nat Cell Biol 2003;5:410–21.
36. Feugaing DD, Tammi R, Echtermeyer FG, et al. Endocytosis of the dermatan sulfate proteoglycan decorin utilizes multiple pathways and is modulated by epidermal growth factor receptor signaling. Biochimie 2007;89:637–57.
37. Joliot A, Trembleau A, Raposo G, et al. Association of engrailed homeoproteins with vesicles presenting caveolae-like properties. Development 1997;124:1865–75.
38. Urbich C, Reissner A, Chavakis E, et al. Dephosphorylation of endothelial nitric oxide synthase contributes to the anti-angiogenic effects of endostatin. FASEB J 2002;16:706–8.

Tumor Cell–Secreted Caveolin-1 Has Proangiogenic Activities in Prostate Cancer

Salahaldin A. Tahir, Guang Yang, Alexei A. Goltsov, et al.

Cancer Res 2008;68:731-739.